Observation of O2 1.27 μm dayglow by SPICAM IR: Seasonal distribution for the first Martian year of Mars Express

Anna Fedorova, Oleg Korablev, Severine Perrier, Jean-Loup Bertaux, Franck Lefèvre, Alexander Rodin

Observation of O_2 1.27 μm dayglow by SPICAM IR: Seasonal distribution for the first Martian year of Mars Express

Anna Fedorova,[1] Oleg Korablev,[1] Severine Perrier,[2] Jean-Loup Bertaux,[2] Frank Lefevre,[2] and Alexander Rodin[1,3]

Received 1 February 2006; revised 16 June 2006; accepted 30 June 2006; published 14 September 2006.

[1] The $O_2(a^1\Delta_g)$ molecule is a result of the photodissociation of ozone in the Martian atmosphere and may be used as a tracer for atmospheric ozone mostly above ~20 km since the singlet delta state is quenched by carbon dioxide at lower altitudes. The SPICAM IR acousto-optic tunable filter (AOTF) spectrometer is a part of the SPICAM experiment onboard Mars Express. It is able to measure the O_2 singlet delta emission band at 1.27 μm with a resolving power of ~2200. We present the first seasonal map of the O_2 emission covering the entire Martian year. Maximal values of O_2 emission are observed during late winter to early spring at high latitudes in both hemispheres. We report the highest dayglow intensity of 30 MR in the southern hemisphere (70°–80°S latitudes) at L_s = 185°–195° and of 26 MR in the north polar regions (latitudes 70°–80°N) at L_s = 10°–20°. The lowest emissions are measured during the southern hemisphere summer near perihelion (L_s = 270°–330°), with an upper limit of 1–2 MR. At low latitudes (30°S–30°N) the seasonal evolution of the O_2 emission shows a distinct maximum (5–7 MR) near aphelion. This is consistent with the maximum in O_3 occurring at this time of the year, which has been reported from Earth, from satellite, or by modeling studies. The comparison of our results with previous measurements carried out from Earth shows quantitative differences that can be attributed to differences in local time of the observation or interannual variability of the Martian ozone layer.

Citation: Fedorova, A., O. Korablev, S. Perrier, J.-L. Bertaux, F. Lefevre, and A. Rodin (2006), Observation of O_2 1.27 μm dayglow by SPICAM IR: Seasonal distribution for the first Martian year of Mars Express, *J. Geophys. Res.*, *111*, E09S07, doi:10.1029/2006JE002694.

1. Introduction

[2] Ozone is a chemically active constituent of the Martian atmosphere formed by the three-body reaction of O_2 and O. Odd oxygen (O_x = O + O_3) budget is partly controlled by the odd hydrogen produced by the photolysis of water vapor and its reaction with $O(^1D)$. Thus measurement of the ozone abundance can be used as a chemical tracer of odd hydrogen species (HO_x). HO_x compounds (with the exception of H_2O_2 recently detected by *Encrenaz et al.* [2004] and *Clancy et al.* [2004] and often related to HO_x because it photodissociates into OH + OH) have never been directly observed on Mars. The knowledge of these odd hydrogen species could be a key to the understanding of the apparent stability of Mars CO_2 atmosphere. The comparison of ozone measurements to atmospheric models should determine the degree of our understanding of Martian photochemistry.

[3] The SPICAM instrument, on board the Mars Express satellite platform, uses several methods for the observation of Martian O_3. The UV spectrometer covers a spectral range of 118–320 nm and it detects O_3 in Hartley continuum near 260 nm (for more details, see *Bertaux et al.* [2001, 2006]). This method allowed ozone detection and the study of its distribution with Mariner and Hubble Space Telescope measurements [*Lane et al.*, 1973; *Wehrbein et al.*, 1979; *Clancy et al.*, 1996, 1999]. Nadir observations by SPICAM UV allow to measure the dayside column abundance of ozone. Star occultation gives a vertical distribution of ozone on the night side of the planet. The third method, sun occultation could give information about morning and evening distribution of ozone.

[4] The near infrared channel of SPICAM allows indirect ozone measurement through observation of the oxygen dayglow $O_2(a^1\Delta_g)$ at 1.27 μm. It is one of the most intense features in the airglows of terrestrial planets, resulting from the (0,0) band of the optical transition of $O_2(a^1\Delta_g - X^3\Sigma^-_g)$. The excited molecule emits a photon if it is not quenched by collision with another molecule. As a result this airglow is more sensitive to high-altitude ozone above ~20 km where the collisional deexcitation is not dominant. The measurement of the intensity of the airglow may be used to infer the concentration of

[1] Space Research Institute, Moscow, Russia.
[2] Service d'Aéronomie, Centre National de la Recherche Scientifique, Verrières-le-Buisson, France.
[3] Moscow Institute of Physics and Technology, Dolgoprudnyi, Russia.

0148-0227/06/2006JE002694

Table 1. Review of Published Ground-Based O_2 Observation From 1973 to 2006 Years[a]

Year of Observation	Ls	Latitude	Longitude	Local Time	Reference
Nov 1973[b]	315				*Noxon et al.* [1976]
May 1975[c]	~230				*Noxon et al.* [1976]
Nov 1975	346	<45S; 20S–20N; >45N			*Traub et al.* [1979]
21 Jan 1997	67.3	50S–90N	52E	14:20	*Novak et al.* [2002], *Krasnopolsky* [2003]
20 Mar 1999	112	60S–90N	subsolar point ~80E sub-Earth point 106E	8:00–18:00	*Krasnopolsky and Bjoraker* [2000], *Krasnopolsky* [2003]
20 Apr 2001	148	75S–80N	subsolar point ~162E sub-Earth point 191E	8:30–17:30	*Krasnopolsky* [2003]
8–12 Jan 2002	306	90S–36N			*Novak et al.* [2005], *Farrell et al.* [2004]
23 Apr 2003	173	80S–60N	subsolar point ~351E sub-Earth point 30E	9:00–18:00	*Krasnopolsky* [2003]
18–24 Mar 2003	155				*Novak et al.* [2005]
11–15 Jan 2004	333				*Farrell et al.* [2004], *Novak et al.* [2005]
2–3 Jun 2005	223				*Novak et al.* [2005]

[a]Observation from 1997 is a part of a large project that began in 1997.
[b]Latitude and longitude: Entire disk of Mars with the averaged local central meridian centered on the Amazonis area.
[c]Latitude and longitude: Entire disk of Mars.

atmospheric ozone if the production and deactivation efficiencies of $O_2(a^1\Delta_g)$ are known. The unit for column-integrated emission is the Rayleigh:

$$1\,\mathrm{R} = 10^6 \big/ \mathrm{photon\,cm^{-2}s^{-1}}(4\pi\,\mathrm{ster})^{-1}$$

[5] SPICAM is not the only instrument aboard Mars Express, capable to observe this emission. Two other spectrometers working in near IR range can observe O_2 dayglow. The short wavelength channel of PFS (Planetary Fourier Spectrometer) works in the range of 1.2–6 μm with a resolution of 1.3 cm^{-1} and the field of view of 1.6° [*Formisano et al.*, 2005]. The spectral resolution of PFS is 2.5 times higher than the resolution of SPICAM (see section 3). Unfortunately, a low signal-to-noise ratio of PFS below 2 μm prevents the measuring of the latitude distribution of the O_2 emission for an individual orbit. However, for an average spectrum taken over a full orbit, the high spectral resolution of PFS permits a study of this band in more detail.

[6] The mapping infrared spectrometer OMEGA works in the range of 0.35–5.1 μm with resolving power of 100 (spectral resolution of 14 nm near 1270 nm) [*Bibring et al.*, 2004]. For this spectral resolution about 98% of the O_2 emission band falls into a single spectral channel at 1271 nm; continuum may be taken in adjacent channels at 1256 nm and 1285 nm. The advantage of OMEGA is its spatial resolution. The mapping spectrometer can produce a map of the emission with a very good spatial resolution, and can provide important details of geographical and vertical (on the limb) distribution.

[7] The SPICAM infrared channel has a resolving power of 2200 at 1270 nm (spectral resolution ~0.55 nm) as well as dependable signal-to-noise ratio, which allows dependable measurements of the $O_2(a^1\Delta_g)$ emission. Measurements of this emission by SPICAM can be compared in the future with other Mars Express data sets, such as those obtained by the OMEGA instrument.

[8] The oxygen dayglow $O_2(a^1\Delta_g)$ at 1.27 μm was predicted after the discovery of ozone in Martian atmosphere by Mariner 7 UV spectrometer [*Barth and Hord*, 1971]. All observations of the O_2 emission before Mars Express were made from the Earth's surface. This dayglow was first detected on Mars by *Noxon et al.* [1976]. Emission was observed at high spectral resolution with the Martian lines Doppler shifted with respect to the telluric lines. The measurements were made independently by two groups led by J.F. Noxon and P. Connes at two different observatories (Mount Palomar and Mount Hopkins). These observations were continued by *Traub et al.* [1979] at the 5-m telescope on Mount Palomar. These latter measurements distinguished among the equatorial region (±20°) and the polar regions (above ±45°) at $L_s = 346°$. The maximum was measured in the North polar region: 26 ± 5 MR, for the South polar region a lower value of 11 ± 2 MR was obtained, and the lowest value was recorded on the equator: 3 ± 1 MR. After a long 20-year gap a new series of ground-based observations of the O_2 emission was carried out by *Krasnopolsky and Bjoraker* [2000], *Novak et al.* [2002], *Krasnopolsky* [2003], as well as *Farrell et al.* [2004] and *Novak et al.* [2005]. These efforts support a project started in 1997 and proposed by *Krasnopolsky* [1997] for mapping the O_2 IR atmospheric band emission on Mars. Observations were made at $L_s = 67°$ in 1997, $L_s = 112°$ in 1999, $L_s = 148°$ in 2001, $L_s = 173°$ in 2003, $L_s = 155°$ in 2003, $L_s = 333°$ in 2004, and $L_s = 223°$ in 2005. In spite of these efforts, the seasonal coverage is still patchy. The summary of the ground-based observations of the O_2 emission is given in Table 1.

[9] In this paper we present oxygen dayglow observations performed during one Martian year by the SPICAM IR spectrometer. After a photochemical theoretical description of the problem in section 2, the description of the IR spectrometer and the retrieval method of the O_2 emission from SPICAM spectra are given in sections 3 and 4. Seasonal distribution and comparison with previous observations are discussed in sections 5 and 6.

2. Oxygen Dayglow at 1.27 μm as a Product of the Ozone Photolysis

[10] There are several ways of formation of the O_2 airglow in the Martian atmosphere. At night, the excitation

of O_2 occurs through the three-body reaction [*Krasnopolsky*, 2003; *Garcia Munoz et al.*, 2005]:

$$O + O + CO_2 \rightarrow O_2(a^1\Delta_g) + CO_2 \quad (1)$$

The column rate of this reaction is 8×10^{10} cm^{-2} s^{-1} in the Martian atmosphere according to *Krasnopolsky* [2003]. The peak of reaction occurs at 50–80 km with an expected airglow column intensity of ~50 kR [*Krasnopolsky*, 2003].

[11] In the daytime, $O_2(a^1\Delta_g)$ is formed in the lower atmosphere of Mars from the ozone photodissociation in the Harley continuum:

$$\begin{aligned} &O_3 + h\nu \rightarrow O(^1D) + O_2(a^1\Delta_g), 200\,\text{nm} < \lambda < 310\,\text{nm} \\ &O_3 + h\nu \rightarrow O(^3P) + O_2(X^3\Sigma_g) \end{aligned} \quad (2)$$

with a quantum yield of 0.9 and 0.1 respectively at wavelengths shorter than 307 nm [*Ball et al.*, 1993; *Ball and Hancock*, 1995]. According to *Nair et al.* [1994], the O_3 photodissociation rate J (s^{-1}) leading to the formation of $O(^1D)$ varies from 1.5×10^{-3} s^{-1} near aphelion to 2.2×10^{-3} s^{-1} near perihelion. These values were used by *Novak et al.* [2002] for their analysis of ground-based observations and were later corrected by *Krasnopolsky* [2003], who obtained J = 7.7×10^{-3} and 5.3×10^{-3} s^{-1} at 1 AU for slant ozone abundances of 0 and 20 μm atm, respectively. These values result in J = 2.9×10^{-3} s^{-1} at aphelion, which differs substantially from the values used by *Novak et al.* [2002]. The J value calculate by three-dimensional model [*Lefevre et al.*, 2004] is 3.4×10^{-3} s^{-1} at 1.52 AU and O_3 = 1 μm atm. It corresponds to 2.75×10^{-3} s^{-1} at aphelion (1.69 AU) and well agrees with Krasnopolsky's value.

[12] From the excited state $O_2(a^1\Delta_g)$ the oxygen molecule can be deactivated through collision or emission. Emission occurs as a result of the transition from $\nu' = 0$ at the excited state:

$$O_2(a^1\Delta_g, \nu') \rightarrow O_2(X^3\Sigma_g, \nu') + h\nu \quad (3)$$

into the vibrational levels $\nu' = 0$ and 1 of the ground electronic state, producing emissions in the near infrared at 1.27 μm (0,0) and 1.58 μm (0,1). The second emission is ~45 times weaker as measured in the laboratory and 70 times weaker as observed in the Earth atmosphere [*Novak et al.*, 2002 and references therein].

[13] In spite of numerous atmospheric studies the radiative lifetime τ of $O_2(a^1\Delta_g)$ is still estimated with a large uncertainty. *Novak et al.* [2002] used τ = 3880 s from *Badger et al.* [1965]. *Krasnopolsky* [2003] indicated a value of 4470 s [see *Lafferty et al.*, 1998]. The value of τ = 4566 s is recommended by *Newman et al.* [1999]. *Mlynczak and Nesbitt* [1995] reported a value of 6803 s, which is ~1.5 times larger than the others.

[14] Deactivation through collision with CO_2 occurs by the following reaction:

$$O_2(a^1\Delta_g) + CO_2 \rightarrow O_2(X^3\Sigma_g) + CO_2 \quad (4)$$

The rate constant for this reaction is very small [*De More et al.*, 1997; *Sander et al.*, 2003], k < 2×10^{-20} cm^3 molecules^{-1} s^{-1}. *Krasnopolsky and Bjoraker* [2000] recommend a value of k = 10^{-20} cm^3 molecules^{-1} s^{-1}. Using constants for appropriate reactions, the equilibrium equation for $O_2(a^1\Delta_g)$ could be written as:

$$\frac{d[O_2(a^1\Delta_g)]}{dt} = J[O_3] - \frac{1}{\tau}[O_2(a^1\Delta_g)] - k[O_2(a^1\Delta_g)][CO_2]$$

Steady state is reached when photochemical equilibrium exists:

$$\frac{d[O_2(a^1\Delta_g)]}{dt} \sim 0, \text{hence}$$

$$J[O_3] \sim \frac{1}{\tau}[O_2(a^1\Delta_g)] + k[O_2(a^1\Delta_g)][CO_2]$$

Where [ ] designate the number density for a given species.

[15] Let us define the emittance $\varepsilon = \frac{[O_2(a^1\Delta_g)]}{\tau}$ as the number of photons emitted from excited state $O_2(a^1\Delta_g)$ per second per cm^3. A remote spectrometer does not measure the emittance directly. It registers the intensity of the emission, i.e., the integral over the line of sight $I = \int \frac{\varepsilon(z)}{4\pi} dz$, where the intensity I is measured in photons/cm^2/s/ster.

[16] The resulting intensity in MR is determined as

$$4\pi I(MR) = \frac{10^{-12} J}{r^2} \int_0^\infty \frac{[O_3]dz}{1 + \tau k[CO_2]}, \quad (5)$$

where J is the ozone photolysis rate coefficient at 1 AU, and r is the Mars to Sun distance in AU.

[17] Because of the deactivation by collision at low altitudes, the contribution of the O_2 emission is more sensitive to high-altitude ozone, i.e., where $\tau k[CO_2] \ll 1$. The relative contribution of lower altitude ozone is smaller than its contribution to ozone column density. The concentration of CO_2 corresponding to $\tau k[CO_2] = 1$ with τ = 4566 s and k = 10^{-20} cm^3 molec^{-1} s^{-1} equal to 2.2×10^{16} cm^3. This value corresponds to the altitudes of 20–26 km depending on the season and latitude. Deactivation through collision with CO_2 dominates below 20 km.

[18] In this paper we present the results of O_2 dayglow measurements, a valuable input for photochemical models, and we do not make an attempt to infer the ozone column abundance. Such an evaluation will be done in the forthcoming study in conjunction with the simultaneous ultraviolet measurements of O_3 also performed by SPICAM [*Perrier et al.*, 2006], to address a vertical distribution of ozone.

3. Measurements

[19] The SPICAM IR spectrometer is a very light (0.8 kg) AOTF (acousto-optic tunable filter) device working in the spectral range 1000–1700 nm. The spectral resolution is roughly constant in wave numbers (~3.5 cm^{-1}), and correspond to 0.55 nm at 1270 nm (resolving power of ~2200). The field of view (FOV) is 1°, which corresponds

to 5–8 km on the surface of the planet for nadir observations at the pericenter of Mars Express orbit. For limb observations the FOV corresponds to vertical extension of 20–80 km depending on the distance from a target to the spacecraft. The noise equivalent brightness of the instrument is ~0.15 W/m^2/micron/ster at 1250–1300 nm. This allows the instrument to reach a high signal-to-noise ratio of 10 to 150 depending on brightness of Mars.

[20] SPICAM is operated in several observation modes: stellar and solar occultations, nadir and limb observations [*Bertaux et al.*, 2006]. These modes differ in the pointing of viewing axis of the instrument. It is the center of Mars for nadir, and the inertial orientation for a limb and a star observation. The O_2 emission was retrieved for nadir observations. We also used stellar occultation measurements and limb observations if the reflected solar light from the surface was observed at a portion of the orbit. We did not retrieve the emission on the limb above the edge of the planet. Such limb measurements are difficult due to large extension of the SPICAM IR FOV on the limb. We will focus here on the integrated emission measured in the nadir or slant geometry.

[21] The AOTF spectrometer operates on a principle of sequential scanning of the spectrum. As a result the measurement of one spectrum takes a certain time. A complete well-sampled spectrum (3984 spectral points from 1 to 1.7 μm) requires 24 sec to be measured. However, during this time the SPICAM FOV footprint on the surface varies by 3° of latitude or ~180 km. Thus changes in the surface albedo and/or aerosol loading during such long measurements may distort the shape of a spectrum. To minimize the potential problem, an optimized, shorter mode of observation allows to record three spectral windows, 996 spectral points in total. These three windows correspond to interesting bands of atmospheric molecules. The first window at 1435–1648 nm covers the main CO_2 bands in the spectral range of SPICAM. The second window at 1340–1440 nm is dedicated to H_2O measurements. The third one at 1258–1287 nm is centered on the O_2 emission. This mode has been routinely operated for nadir and limb observations from orbit 134 (L_s = 353°, 21 February 2004). With the optimized treatment the time required to measure one spectrum is only 6 sec. The observation modes of the SPICAM IR spectrometer are described in detail by *Korablev et al.* [2006].

[22] For the retrieval of the O_2 emission intensity we used observations performed from January 2004 to November 2005. In order to increase the signal-to-noise ratio most of data were averaged by groups of 16 spectra. In the beginning of the mission (orbits 8–103, L_s = 330°–345°), due to a larger noise of the IR spectrometer that was not operated yet in optimized mode, data were averaged over 20 spectra.

[23] The calibration of the SPICAM IR spectrometer was performed on the ground and in flight. The absolute calibration of spectra is critical to the analysis of the O_2 emission. The most accurate absolute calibration of SPICAM was obtained in flight by comparing with measurements performed simultaneously by the OMEGA mapping spectrometer on Mars Express [*Bibring et al.*, 2004]. The accuracy of OMEGA calibrations is better than 15%. The description of SPICAM IR calibration is given in a paper by *Korablev et al.* [2006].

[24] To illustrate the main spectral signatures observed together with the O_2 emission we will consider three typical spectra. Three SPICAM spectra recorded in the windows including the H_2O, CO_2 and O_2 bands are presented in Figure 1. The curves correspond to different seasons and locations on Mars. Curves 1 and 2 were recorded on orbit 262 (L_s 13.3°) and correspond to the northern hemisphere spring. At 34° of latitude the O_2 emission is weak, and does not exceed 3 MR. Other features are the signatures of CO_2 gas at 1430–1450 and 1570–1620 nm, and the H_2O vapor band at 1350–1400 nm. In contrast, a much stronger O_2 emission is observed at high latitudes (curve 2). The shape of this spectrum is dominated by a broad H_2O ice signature from 1350 to 1650 nm. Curve 3 is a spectrum recorded above South Pole on orbit 1920 (L_s = 249°). In this case, the strong signature of CO_2 ice [*Hansen*, 2005] contaminates the O_2 emission band and prevents the accurate estimation of its intensity (see section 4.1).

4. Retrieval Technique

4.1. Spectrum of O_2 Emission Measured by SPICAM IR

[25] The spectral window dedicated to the detection of the O_2 emission covers the 1258–1287 nm interval. Let us consider in detail the features observed in this window in the three spectra already presented in Figure 1. To facilitate the comparison, the spectra in Figure 2 are normalized at 1250 nm (continuum portion of the spectrum). Curve 1 corresponds to the spectrum recorded in northern midlatitudes when the O_2 emission is negligible. Curve 2 represents a spectrum recorded by SPICAM IR near the North Pole (orbit 262, L_s 13.3°) where a strong O_2 dayglow emission feature is apparent. Curve 3 corresponds to a spectrum near the South Pole in the spring. This spectrum reveals strong signatures of CO_2 ice on the surface of Mars (see Figure 1). A weak narrow feature of the CO_2 ice falls into the spectral range of 1264–1270 nm (see section 4.4). The depth of this contaminating feature depends on the amount of the CO_2 ice, and the presence of the CO_2 ice on the surface (or in the atmosphere) prevents the accurate measurement of the O_2 emission.

[26] To obtain the absolute intensity of the O_2 emission we need to consider all the spectral features in the range of interest. Solar Fraunhofer lines and some weak CO_2 gas absorption lines are always present in the range of 1260–1285 nm. The absorption by water vapor is negligible.

[27] A theoretical solar spectrum [*Fiorenza and Formisano*, 2005] convolved by the SPICAM resolution is presented in Figure 2. Solar lines are visible at 1264, 1265, 1268 nm and can be a source of error if not properly accounted for. In particular, the line at 1268 nm is located near the maximum of the O_2 emission. To minimize the uncertainties associated to the theoretical solar spectrum we constructed a reference spectrum from SPICAM data, using measurements where the O_2 emission is not present. The method to construct such a reference spectrum is described in section 4.3 in detail.

[28] To estimate the influence of the CO_2 absorption, we calculated a model transmittance of CO_2 gas for a surface pressure of 8 mbar (Figure 3). Spectra are computed with a temperature profile corresponding to northern hemisphere

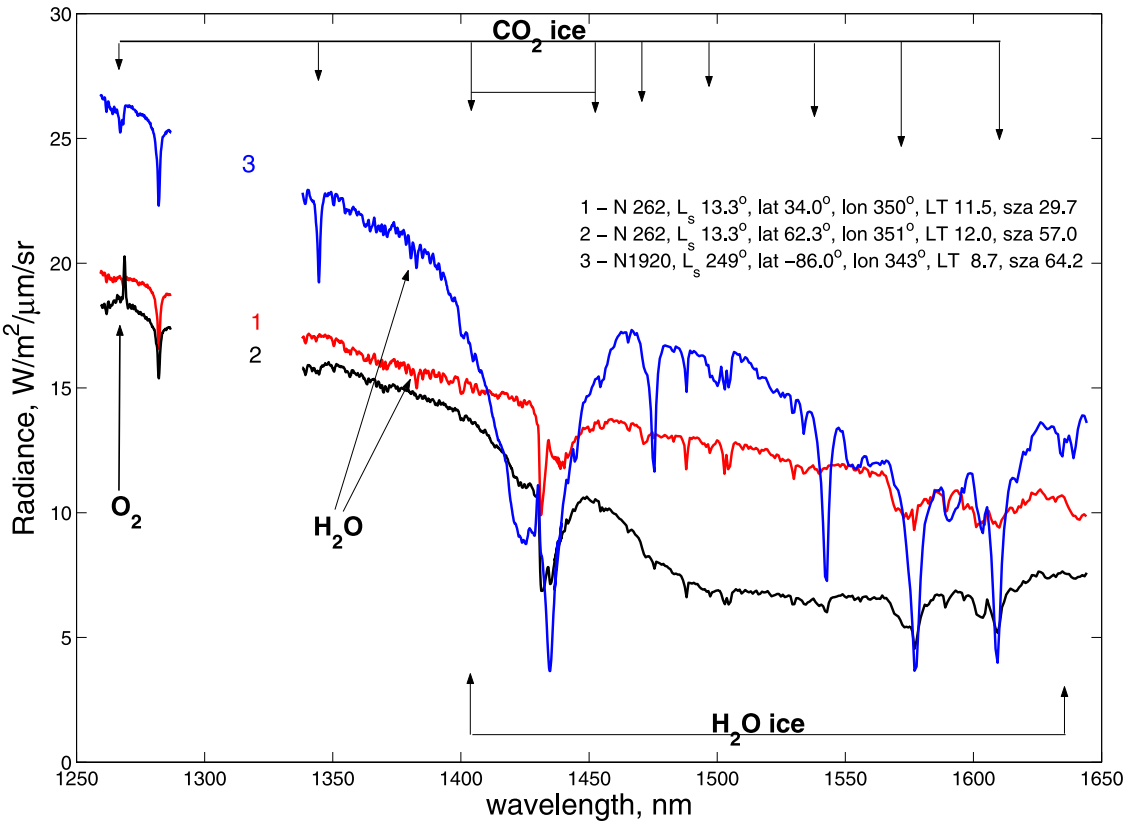

Figure 1. Examples of IR spectra recorded by SPICAM at L_s = 13.3° (orbit 262) and L_s = 249° (orbit 1920). Each of the three spectra consists of three windows: 1435–1648 nm, 1340–1440 nm, and 1258–1287 nm. The first two windows are adjacent, but the spectral sampling is different: fine for the H_2O absorption region and coarser for the rest of the spectrum. Curve 1 is a spectrum recorded at L_s = 13.3° and 34°N, for which O_2 emission is very weak. Absorption is visible in the CO_2 bands at 1430–1450 and 1570–1620 nm and in the H_2O vapor band at 1350–1400 nm. Curve 2 is a spectrum recorded at L_s = 13.3° and 62.3°N, revealing a strong (~23 MR) O_2 emission and a broad signature of H_2O ice at 1400–1650 nm. This is the season of maximum O_2 emission in the northern polar region. Curve 3 is a spectrum recorded at L_s = 249° and 86°S. Strong sharp signatures of the CO_2 ice are apparent as well as water vapor absorption. N, the number of orbit; lat, latitude; lon, longitude; L_s, areocentric solar longitude; LT, local time; SZA, solar zenith angle.

summer (L_s 100°) and to latitude of 70°N, taken from the EMCD database [*Forget et al.*, 1999]. Spectroscopic parameters of CO_2 lines are taken from HITRAN 2004 [*Rothman et al.*, 2005]. Dust is not taken into account. Two values of air mass M = 2, and M = 6 are considered. Air mass M characterizes the optical path in the atmosphere: $M = \frac{1}{\mu_s} + \frac{1}{\mu_o}$, where μ is cosine of observation angle and μ_o is cosine of solar zenith angle. This simulation shows that CO_2 absorption below 1270 nm does not exceed 0.6% for air mass 2 and 2% for air mass 6. The air mass M = 2–4 is typical for SPICAM nadir observation.

[29] The impact of the CO_2 absorption is illustrated by another theoretical curve in Figure 2, which represents a solar spectrum multiplied by CO_2 transmittance for air mass M = 2. To minimize uncertainties due to CO_2 absorption we restricted the spectral range for the retrieval of the O_2 emission to 1267.5–1275 nm, free from the CO_2 absorption.

4.2. Synthetic Spectrum of the O_2 Emission

[30] For the identification of the electronic vibrational ($a^1\Delta_g - X^3\Sigma^-_g$) (0,0) bands of the O_2 molecule, we used the HITRAN 2004 database [*Rothman et al.*, 2005]. The lines of $a^1\Delta_g - X^3\Sigma_g$ transition are located in the range 1250–1290 nm with a maximum around 1268 nm. Line intensities depend on the temperature of the atmospheric layer where the emission occurs. Some attempts to determine the rotational temperature of the O_2 emission were performed from Earth-based observations. The early study of *Noxon et al.* [1976] mentioned rotational temperature of 200–230 K. *Traub et al.* [1979] obtained temperatures of 152–211 K varying with location and time of observation. From recent observations [*Novak et al.*, 2002] the temperature of the atmosphere relevant to the emission is estimated to 175 K. General circulation models [*Forget et al.*, 1999] predicts temperatures within the 140–210 K range at altitudes of 20–40 km. We have therefore chosen an average value of the temperature corresponding to O_2 emission of 175 K.

[31] We did not try to retrieve the rotational temperature from the O_2 emission band from SPICAM spectra. We estimate the error of such retrieval to be as much as 30 K.

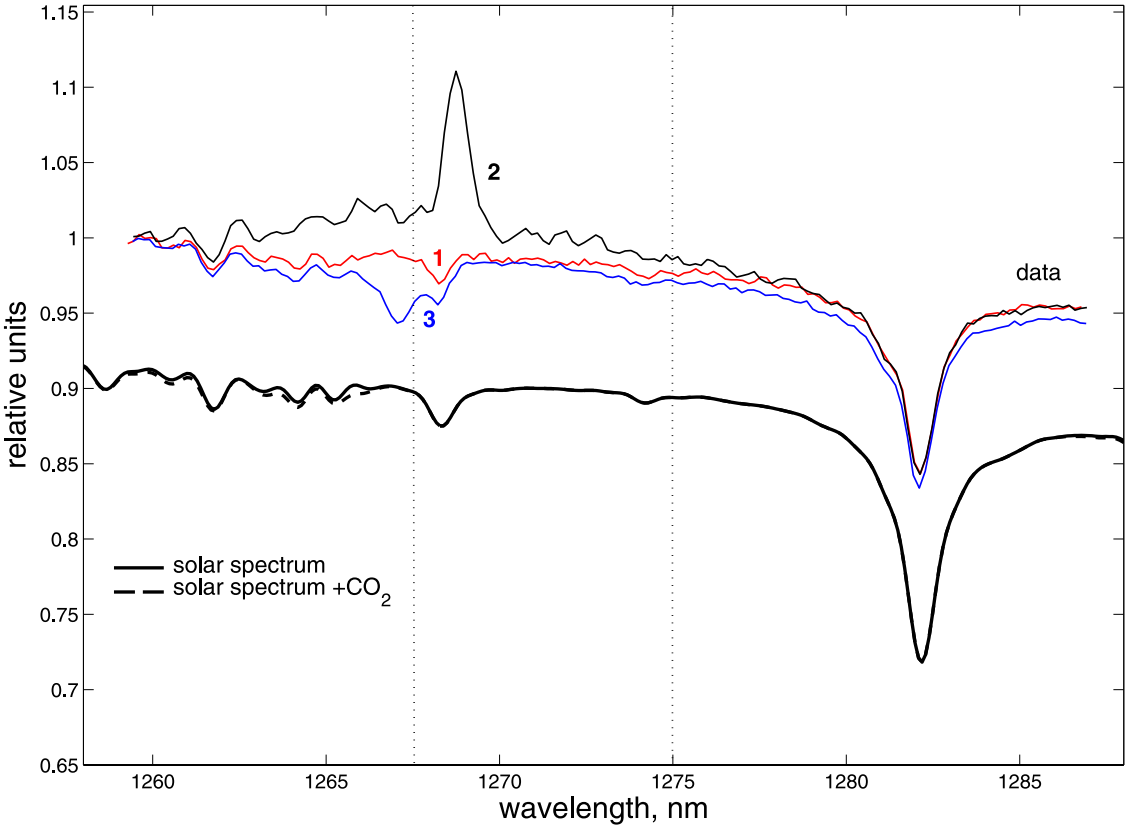

Figure 2. Same as Figure 1, focused on the O_2 emission band and normalized at 1250 nm (thin curves). A strong emission is observed for curve 2, in contrast with curves 1 and 3, which show no noticeable O_2 signature. Note a weak absorption feature of CO_2 ice on curve 3 (1262–1269 nm). The thick curve is the solar spectrum [*Fiorenza and Formisano*, 2005]. The features at 1262, 1268, and 1282 nm are clearly identified as solar lines. Thick dashed line is the solar spectrum modified by CO_2 atmospheric absorption for air mass 2. The spectral range used for the retrieval is marked by dotted lines.

Unlike high-resolution Earth-based measurements, SPICAM cannot resolve separate rotational lines to produce a reliable analysis of the rotational temperature.

[32] Following *Krasnopolsky and Bjoraker* [2000] the intensity of the O_2 emission lines can be calculated as:

$$I_k(T) = AS_k(T)\nu^3 \exp\left(-\frac{h\nu}{kT}\right), \quad (6)$$

where $S_k(T)$ is the strength of the k line at temperature T. A is the proportionality factor; ν is a frequency of transition. The intensities of individual lines (Figure 4, top) are calculated using equation (6) for T = 175 K with line strengths from HITRAN 2004. Then we converted it to Voigt profile and spectral resolution of SPICAM, and scaled to the value of O_2 emission on Mars. Resulting theoretical emission spectra are shown in Figure 4 (bottom) for integrated O_2 emissions of 2, 6, and 20 MR. We neglect self-absorption of O_2 in the Mars atmosphere because of the small O_2 abundance.

4.3. Reference Spectrum and Estimation of Emission

[33] To estimate the emission from the SPICAM data we converted all calibrated spectra from W/m^2/μm to MR/nm (example of spectra are presented in Figures 5, 6, and 7):

$$4\pi \mathrm{I(MR/nm)} = 4\pi * 0.503 * \mathrm{F}\left(\mathrm{W/m^2/\mu m}\right) \times \lambda(\mu\mathrm{m}) \quad (7)$$

[34] To construct the reference spectrum from SPICAM data we use measurements for which the O_2 emission is not present. On the orbit 2247, corresponding to L_s = 305° and 35°–50°S latitude the value of the emission could not exceed 1 MR. This is consistent with general circulation model calculations which predict very small ozone amount near perihelion in the southern hemisphere [*Lefevre et al.*, 2004]. We averaged 40 spectra on this orbit to obtain the reference spectrum (dashed curves in Figures 5 and 6). Average pressure for this spectrum is 4.6 mbar (from the Mars GCM database [*Forget et al.*, 1999]), and average air mass M = 2.2. The reference spectrum is the spectrum of reflected solar radiance passed through Mars atmosphere in the above conditions, and it corresponds to a fixed CO_2 content and local surface albedo:

$$I_{\mathrm{ref}} = I_{\mathrm{sun}} A_{\mathrm{ref}} \mu_{\mathrm{ref}} \exp(-\tau_{\mathrm{ref}} M_{\mathrm{ref}}), \quad (8)$$

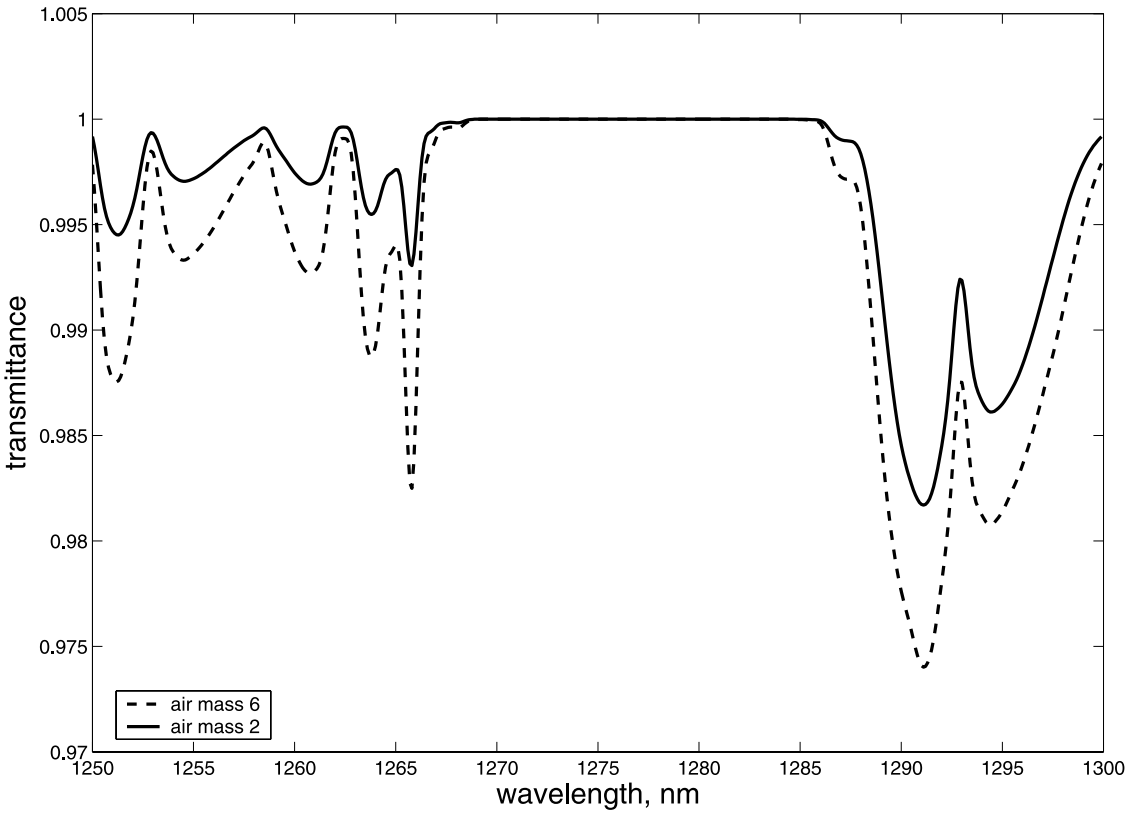

Figure 3. Synthetic spectra of CO_2 transmittance calculated for a surface pressure of 8 mbar and a climatological temperature profile for $L_s = 100°$, latitude of 70°N, and two different air mass factors. The atmosphere is assumed free of dust or clouds.

where I_{sun} is the solar radiance, A_{ref} is the surface albedo for the reference spectrum, μ_{ref} is the cosine of observation angle, τ_{ref} is the column optical depth of gaseous absorption, M_{ref} is the air mass. For different conditions we can define another reference spectrum I_i:

$$I_i = I_{sun} A_i \mu_i \exp(-\tau_i M_i), \tag{9}$$

Gas absorption τ_i in this case can be calculated using an average surface pressure and temperature profile from the GCM database for reference spectrum season, local time, latitude, longitude, and observation geometry. Only the CO_2 absorption is taken into account. Dividing equation (9) by (8) allows to obtain the reference spectrum for any spectrum recorded by SPICAM:

$$I_i = I_{ref} k_i^{alb} k_i^{co2}, \tag{10}$$

where the correction factor $k_i^{co2} = \exp(\tau_{ref} M_{ref} - \tau_i M_i)$ accounts for gas absorption, and $k_i^{alb} = A_i/A_{ref}\ \mu_i/\mu_{ref}$ accounts for the continuum.

[35] To avoid recalculation of the gaseous correction factor k_i^{co2} for each spectrum we use only the spectral range of 1267.5–1275 nm (Figure 2) to integrate the measured intensity of the O_2 emission. This interval is free from the CO_2 absorption, but it covers only a portion of the full range of O_2 emission (see Figures 5 and 6). Using the theoretical spectrum of the Martian (0,0) band computed by the procedure described above (equation (6) and Figure 4), we can estimate that the intensity of the band in this range corresponds to 0.512 from the full intensity of the band at 175 K. This fraction slightly changes with temperature from −0.5% to +1.1% for 140 K and 210 K respectively.

[36] To fit the continuum for each individual spectrum, corresponding to different surface albedo we scale the reference spectrum at 1258 and 1285 nm. At 1285 nm, there is no O_2 emission (see Figure 4) and we see the real continuum. However, at 1258 nm the residual O_2 emission is still present, that could be a potential source of error.

[37] To calculate the O_2 emission measured by SPICAM we integrate the difference between the measured spectrum and the reference spectrum in the spectral range 1267.5–1275 nm, and then divide the retrieved value by the factor of 0.512 (Figures 5 and 6).

[38] To obtain the emission value scaled to the vertical atmospheric column we need to correct for air mass and surface reflectance taking into account the vertical distribution of the emitting layer. Following *Krasnopolsky* [2003] we used the formulation

$$4\pi I = \frac{4\pi I_m}{\frac{1}{\mu} + 2\rho}, \tag{11}$$

where $\rho = \frac{\pi I_{cont}}{I_{sun}\mu_o}$ is the reflectance for an individual spectrum, $4\pi I_m$ is the measured intensity, I_{sun} is the solar radiance corrected by the heliocentric distance, and I_{cont} is the continuum intensity.

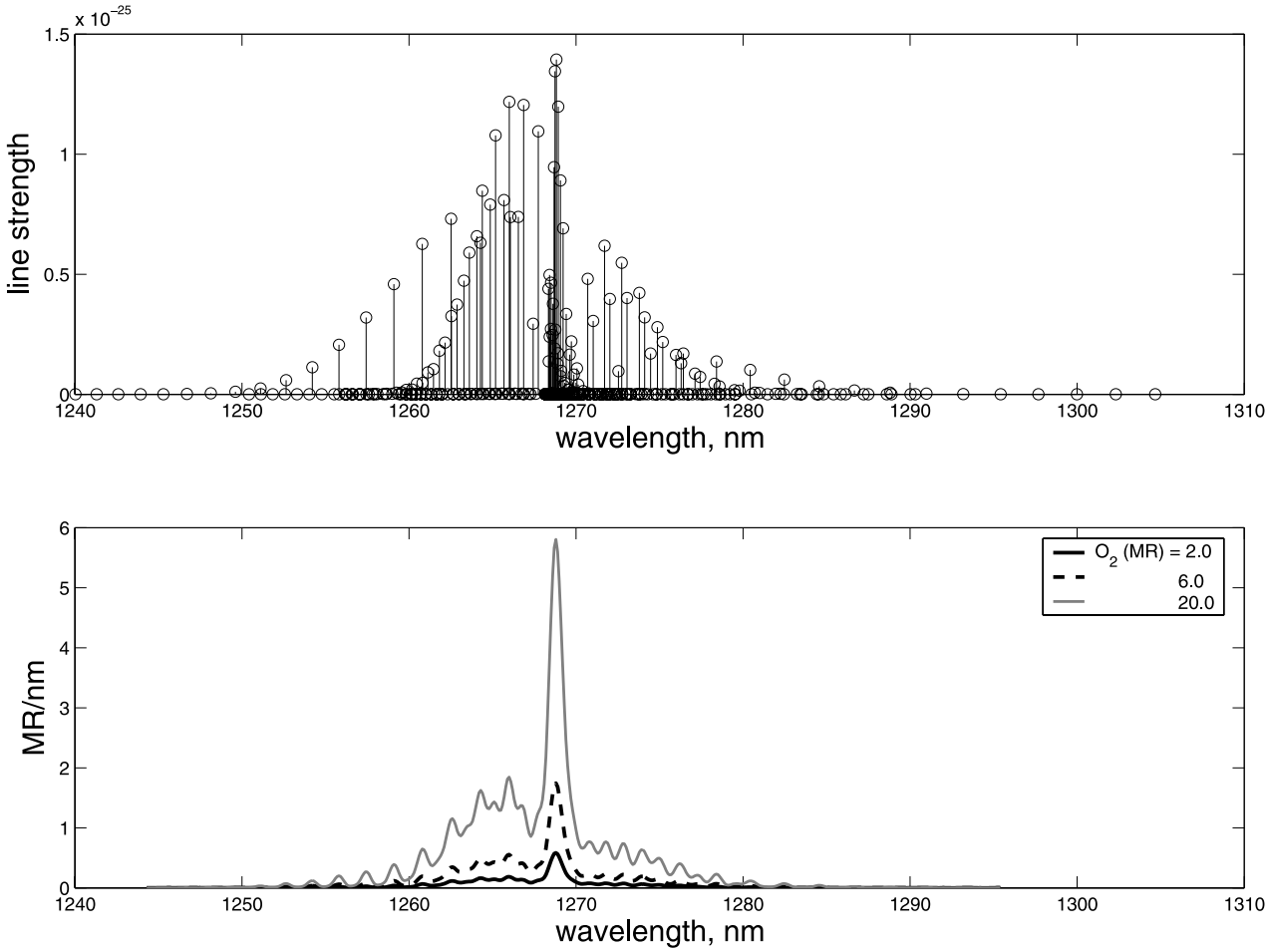

Figure 4. (top) Line strengths of $O_2(a^1\Delta_g)$ band from the HITRAN 2004 spectroscopic database [*Rothman et al.*, 2005] and a temperature of 175 K. (bottom) Synthetic spectra of the O_2 emission converted to the SPICAM IR resolution.

[39] The obtained O_2 emission map is plotted in Figure 8 as a function of the season and is discussed in section 5.

4.4. Error Analysis

[40] The random error of SPICAM measurements depends on the instrument noise. The noise equivalent brightness (NEB) of SPICAM IR equals to 0.15 W/m^2/ μm/ster [*Korablev et al.*, 2006] which corresponds to 1.2 MR/nm at 1.27 μm (equation (7)). This value is two times larger than the maximum of emission at 1269 nm for 2 MR and 1.3 times smaller than the emission maximum for 6 MR. Averaging 16 spectra reduces the noise of an individual spectrum point to 0.3 MR/nm. Taking into account the noise of the reference spectrum (obtained by averaging 40 spectra), the error for each spectral point increases to 0.36 MR/nm. In the 1267.5–1275 nm range there are 42 spectral points characterizing the O_2 band. Averaging these points weighted by the theoretical emission intensity, and taking into account the spectral sampling of 0.18 nm, results in an uncertainty of the measured band intensity of 0.42 MR. As we measure only a portion of the band which accounts for 0.512 of the total band intensity (see section 4.3), the error for the entire band is 0.82 MR, which we round to 1 MR.

[41] This random error characterizes the uncertainty of the measured emission, and should be scaled down according to equation (11) when computing the emission of the vertical atmospheric column.

[42] Other errors are of systematic origin. The most important is the uncertainty in the absolute calibration of SPICAM (15%, see section 3). This uncertainty is directly translated to the measured intensity. An important source of systematic errors is the contamination by the CO_2 ice absorption (Figure 7). In South polar regions at L_s 180°–250° the surface CO_2 ice is observed almost everywhere. The CO_2 ice band masks the O_2 emission completely if the intensity is small. For stronger airglow CO_2 ice may cause an underestimation of the O_2 emission due to the deformation of the continuum. Another source of errors is a systematic shift of 4–5% due to uncertainty in the reconstruction of the continuum. The error due to the CO_2 absorption is weak, and vanishes completely due to appropriate choice of the spectral range. Concluding, the most important sources of error are the uncertainty of absolute calibration, and the contamination by CO_2 ice. Note that CO_2 ice contamination affects not only SPICAM measurements, but all moderate to low spectral resolution observa-

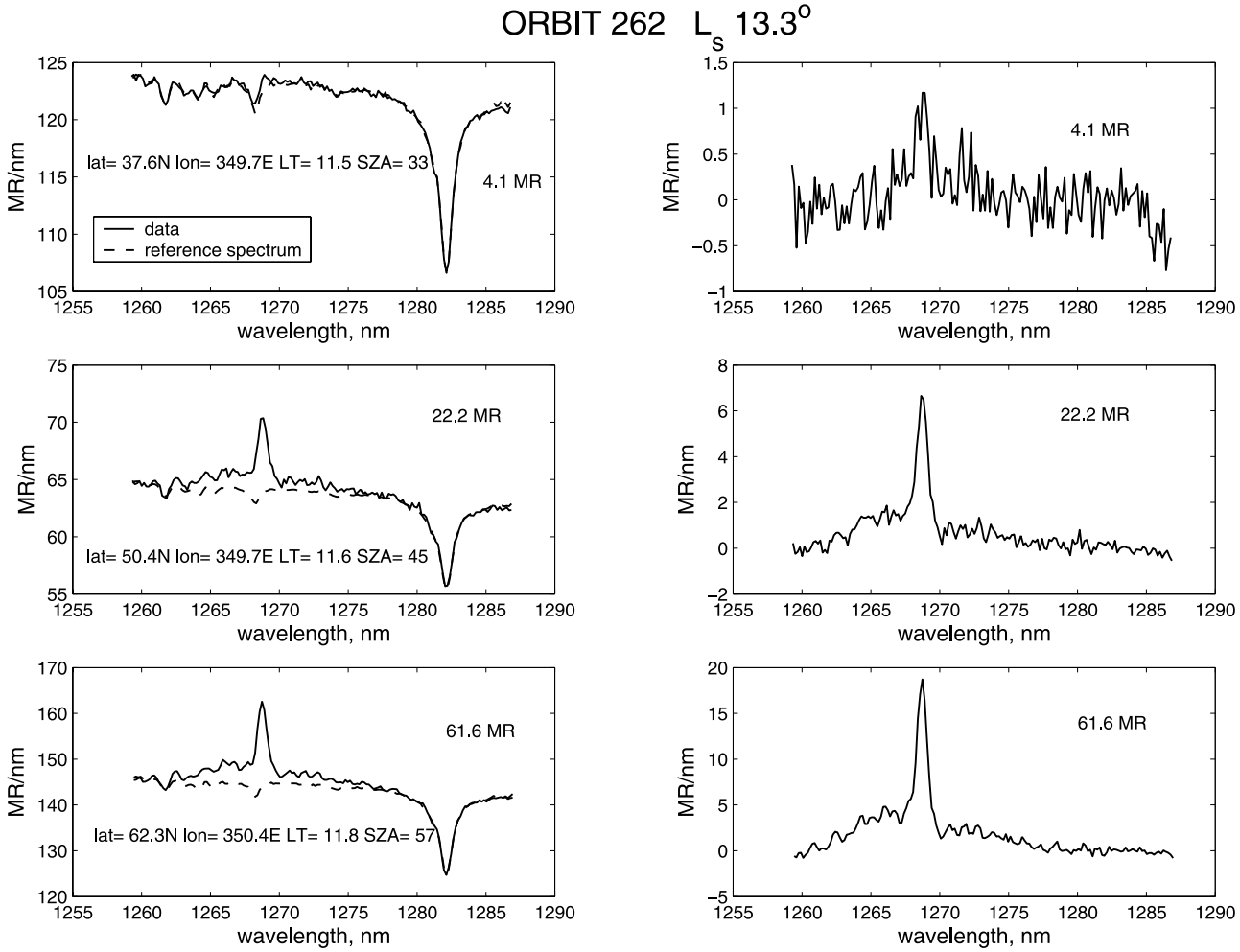

Figure 5. (left) Estimations of the O_2 emission using the reference spectrum (dashed line). Three example spectra from orbit 262 are shown. To obtain the value of the emission, we integrate (right) the difference between the two spectra in the range of 1267.5–1275 nm and correct for the missing part of the band (see text). The emission magnitudes shown here are not scaled by air mass and surface brightness.

tions of O_2 emission. Earth-based high-resolution observations are not sensitive to such contamination.

[43] Dust and clouds can also affect the retrieval of the O_2 emission in the infrared. *Novak et al.* [2002] pointed out that the local minimum observed at 20°–30°N and L_s = 67° might be explained by the aphelion cloud belt. The O_2 dayglow originated mostly from the region above 20 km, while in most cases the dust is confined below 20–25 km, and its effect is minimal. However, one might expect the influence of dust near perihelion during the dust storm season [*Smith*, 2004]. High-altitude hazes are also present on Mars [*Jaquin et al.*, 1986; *Montmessin et al.*, 2006] and can affect the measurement of the O_2 emission intensity. In the present work we do not correct the O_2 emission for the presence of dust and clouds.

[44] The equation (11) is inapplicable to limb measurements and large observation angles, for which cosines of emission and solar zenith angles approach zero. Furthermore, in this case neglecting dust extinction becomes questionable. To avoid additional uncertainties data obtained at solar angles larger than 85° are discarded in our analysis.

[45] The random detection threshold of 1 MR should not prevent SPICAM from detecting of the O_2 nightglow induced by the three-body reaction (equation (1)). The expected intensity is ~50 kR [*Krasnopolsky*, 2003; *Garcia-Munoz et al.*, 2005], which corresponds to 1–2 MR at the limb. However, SPICAM has a large FOV in this configuration and requires a long time to measure one spectrum. At the altitude of the emission (50–80 km) only 1–3 spectra can be recorded, and we estimate the possibility for the O_2 nightglow as marginal.

5. Seasonal Distribution of O_2 Emission

[46] The distribution of the O_2 emission measured by SPICAM IR over the first Mars Express Martian year from L_s = 330° (January 2004) to L_s = 327° (November 2005) is shown in Figure 8. We used data from 780 orbits, and results are zonally averaged into bins of 2° in latitude and 1° in L_s. Data are missing in the L_s = 75°–90° interval when

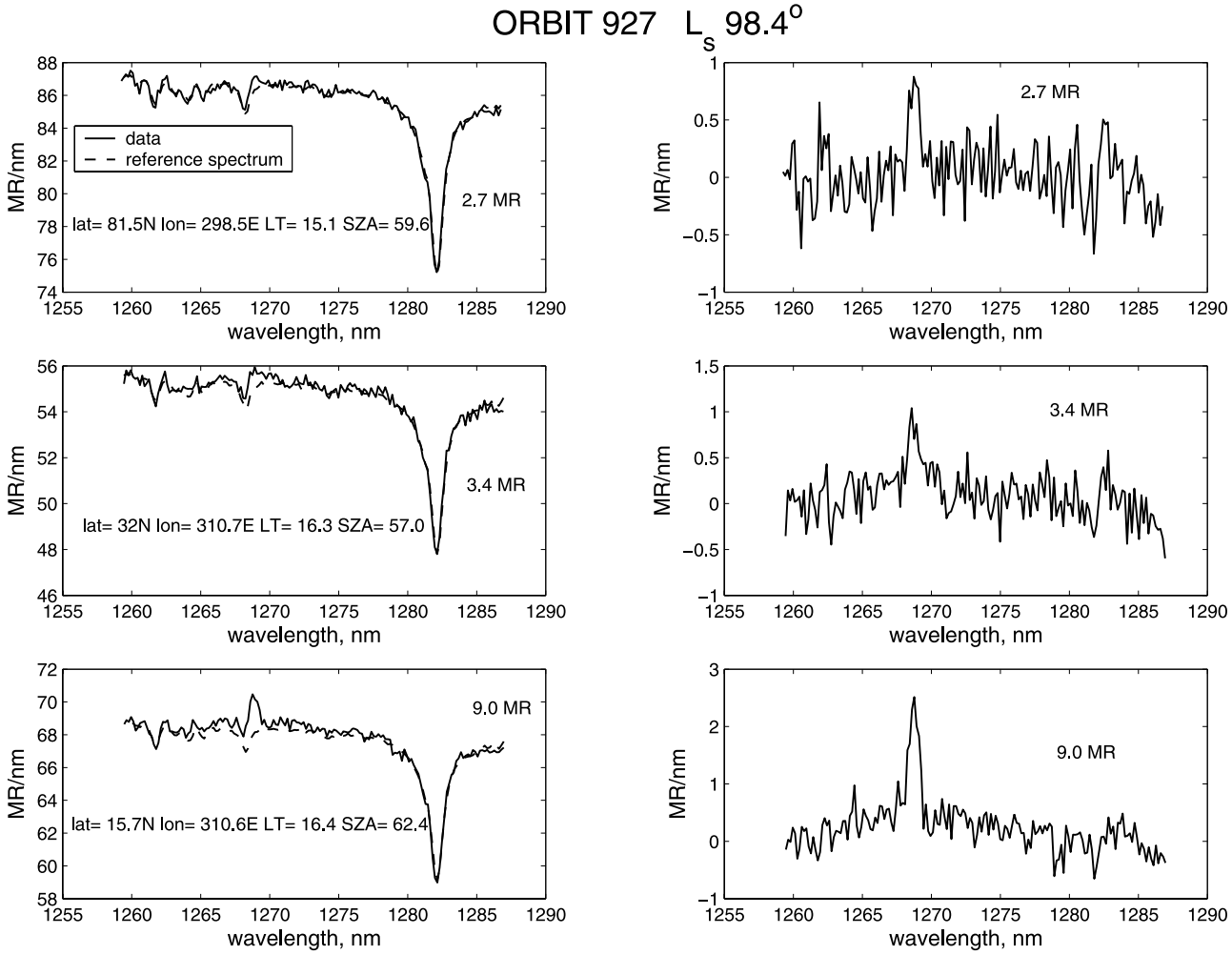

Figure 6. Same as in Figure 5 but for orbit 927 (Ls = 98.4°).

the pericenter of Mars Express was on the night side. SPICAM observations could not be performed in the L_s = 200°–240° period due to the antenna deployment of the MARSIS instrument. In addition, SPICAM observations are generally restricted to the sunlit part of the planet, and thus no nadir data are obtained during the polar night.

[47] The largest O_2 emissions are observed at high latitudes in early spring. Maxima of 26 MR are measured near the North Pole at L_s = 0°–20°, and reach 30 MR at L_s = 185°–195° in the southern hemisphere. There is also evidence of substantial O_2 emissions near fall equinox in both polar regions. In the northern hemisphere, a strong maximum is observed around L_s = 180° with emissions up to 18 MR. A similar phenomenon is detected in the southern hemisphere, where emissions of the order of 15 MR are measured shortly after fall equinox at L_s = 20°–40°. Two peaks at spring and fall equinoxes are generally consistent with 3D model, except the O_2 emission in spring in the southern hemisphere that looks higher than the model prediction [*Levefre et al.*, 2004].

[48] At low latitudes (30°S–30°N), the evolution of the O_2 emission monitored by SPICAM shows a distinct maximum centered on aphelion, with about 5–7 MR measured between L_s = 30° and L_s = 90°. In contrast, the emission observed during the rest of the year at those latitudes is weak and is in general smaller than 3 MR. At L_s = 210°–240° a small emission of ~2–3 MR is still detected at the South Pole. However, because of contamination of spectra with the CO_2 ice feature (see above) the O_2 emission at the South Pole could be overestimated. At L_s = 270°–330° the emission is very weak at high southern latitudes, as compared to other seasons. The value does not exceed 2 MR on the average.

[49] The results presented here are consistent with the O_3 measurements performed in the ultraviolet by SPICAM [*Perrier et al.*, 2006] and with three-dimensional model simulations [*Lefevre et al.*, 2004]. Maximum ozone abundances on Mars are known to occur at high latitudes in winter. This is explained by the cold polar temperatures that result in the freezing out of water vapor, and prevent the formation of the ozone-destroying hydrogen radicals. The maximum $O_2(a^1\Delta_g)$ emission observed by SPICAM at the spring and fall equinoxes, before and after the polar night, confirms the presence of large ozone abundances in the wintertime polar regions. At low to middle latitudes, the orbital ozone variations are believed to be driven by the water vapor saturation level (hygropause) altitude in middle atmosphere [*Clancy and Nair*, 1996]. Around aphelion, the cold and dust-free atmosphere leads to a low hygropause (10–15 km), with rapidly decreasing H_2O mixing ratio

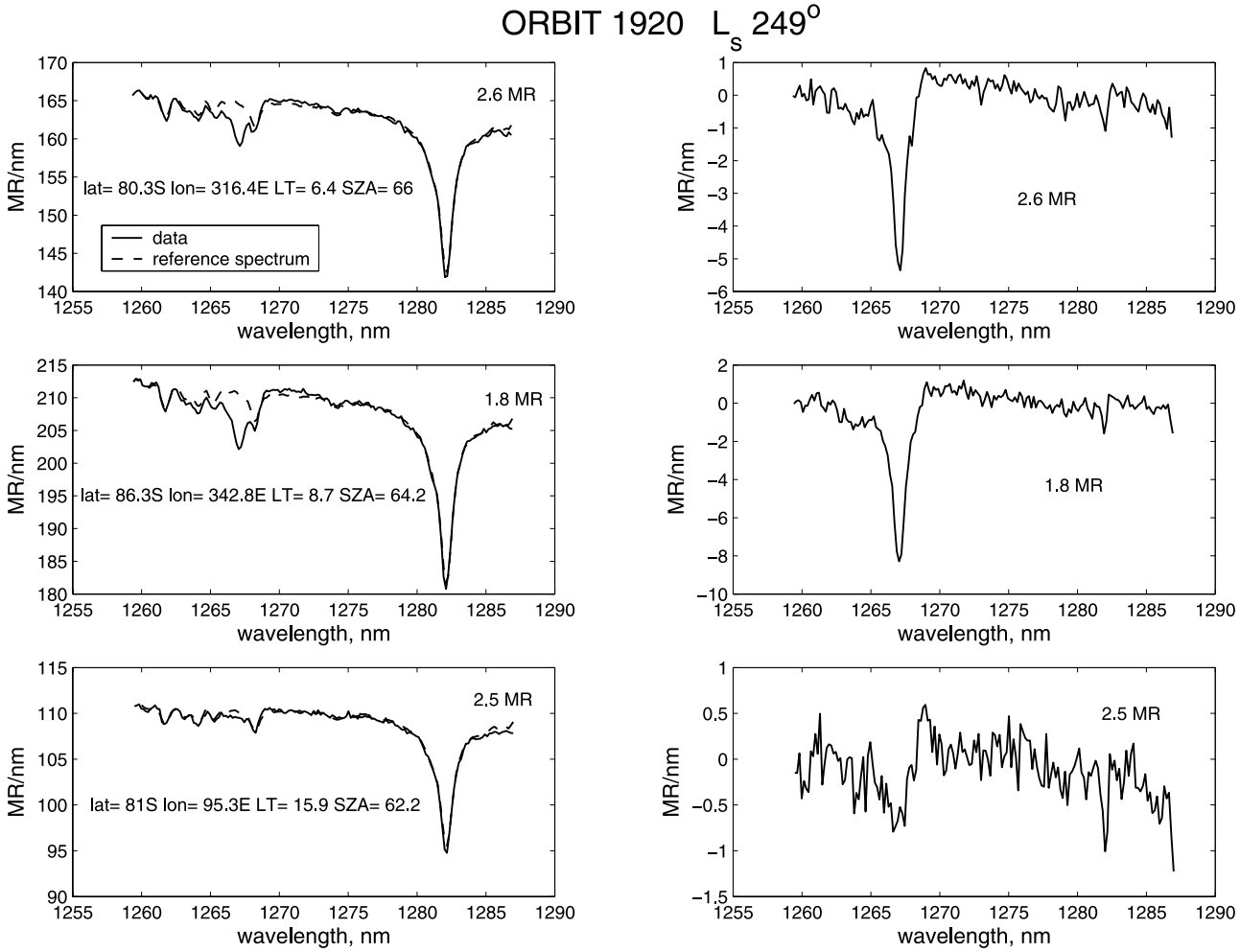

Figure 7. Same as in Figure 5 but for orbit 1920 (L_s 249°), corresponding to the south pole region in spring.

above the hygropause. This favors the formation of the so-called O_3 "aphelion layer" above 20 km, predicted by model simulations [*Lefevre et al.*, 2004] and observed in the ultraviolet by stellar occultation with SPICAM [*Lebonnois et al.*, 2006]. The $O_2(a^1\Delta_g)$ emission is sensitive to the high-altitude O_3 increase during the aphelion season. The enhanced emission that we observe at low latitudes between L_s = 30° and L_s = 120° gives a new independent indication of this O_3 increase, already noted from Earth [*Clancy et al.*, 1999; *Fast et al.*, 2006a] or from SPICAM in the ultraviolet [*Perrier et al.*, 2006].

[50] Figure 9 plots the orbital evolution of the O_2 emission intensity at the equator and for high latitudes (65°S, 65°N). The increase in emission in the equatorial region is clearly visible at L_s = 30°–120°, with a maximum of 5 MR. In contrast, the intensity measured at low latitudes does not exceed 1–2 MR for the rest of the year. At high latitudes, Figure 9 clearly shows the peak in O_2 emission measured around equinoxes in both hemispheres. The emission is minimum in summer, the northern summer minimum (4 MR) being less pronounced than the southern summer minimum (1–2 MR). This seasonal asymmetry of the summer minimum, which is not as evident in terms of total ozone [*Perrier et al.*, 2006], could be connected to the variations in the H_2O saturation altitude. Detailed comparisons of ozone, $O_2(a^1\Delta_g)$ emission, and water vapor measurements by SPICAM will be the subject of a forthcoming study supported with appropriate three-dimensional model simulations.

6. Comparison With Other Data Set

[51] The O_2 emission is directly related to the O_3 photolysis and hence should have a strong variation with local time. *Krasnopolsky and Bjoraker* [2000] and *Krasnopolsky* [2003] pointed out the strong diurnal variation of the $O_2(a^1\Delta_g)$ emission, peaking at noon (12–14 h), this was further demonstrated in the reference to *Farrell et al.* [2004]. However, there is much more ozone at night [*Lefevre et al.*, 2004; *Lebonnois et al.*, 2006]. In the case of Mars Express polar orbit, the local time of nadir observations is slowly changing from one orbit to another. Thus measurements obtained in different seasons correspond in general to different local times (Figure 10), and this must be taken into account when comparing SPICAM data with other observations.

[52] Below we compare our measurements with ground-based observations of the O_2 emission. We do not compare

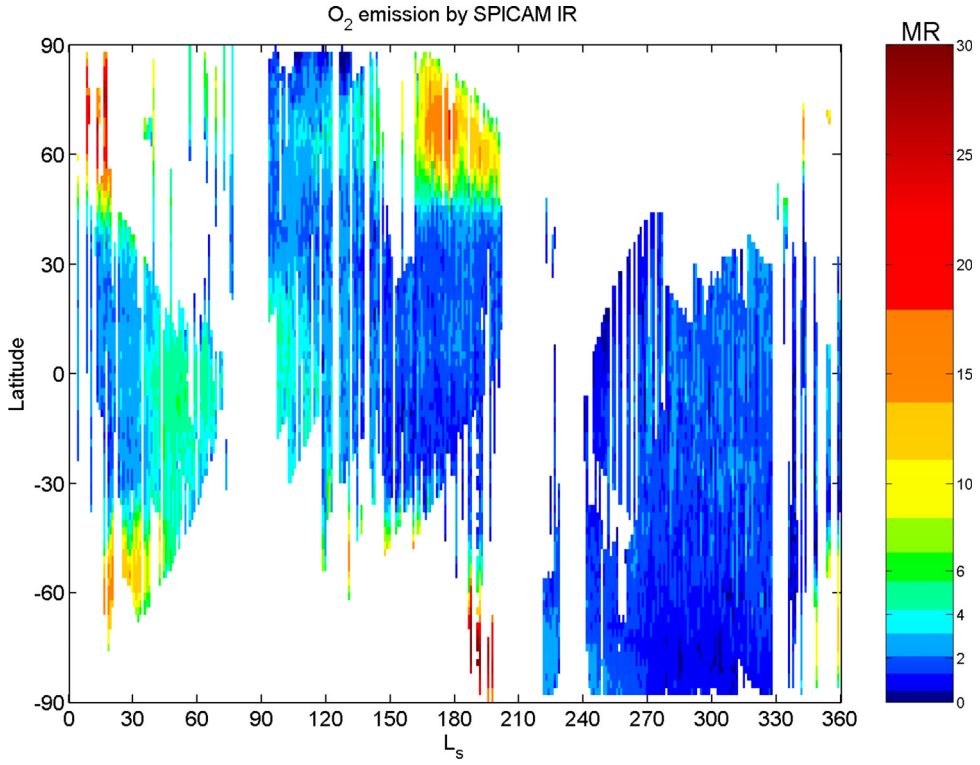

Figure 8. Seasonal distribution of the O_2 emission observed by SPICAM from L_s 330° (January 2004) to L_s 327° (November 2005).

with spacecraft and ground-based ozone measurements, referring to paper by *Perrier et al.* [2006]. Measurements performed by *Traub et al.* [1979] at L_s = 346° indicate a maximum in the northern polar region: 26 ± 5 MR, a lower value of 11 ± 2 MR for the South polar region, and 3 ± 1 MR on the equator. Our coverage is not very good for this season. One orbit at L_s = 343° indicates a maximum of 15 MR at 60°–80°N, which is a little smaller than 26 MR obtained from the Earth. In the 50°–80°S latitude band our measurements made at L_s = 348° indicate an emission of about 10 MR, in good agreement with that by *Traub et al.* [1979]. The minimal emission (below 2 MR)

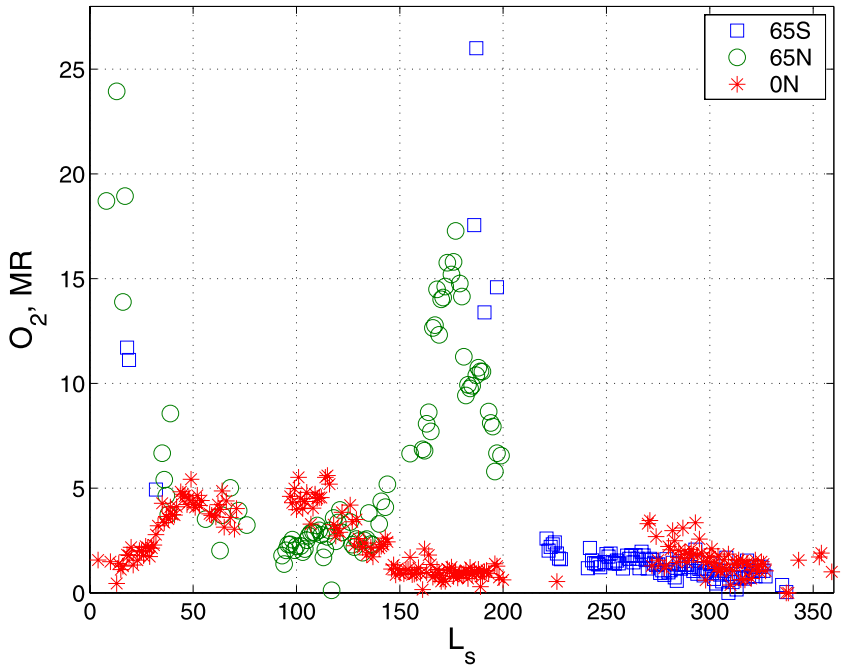

Figure 9. Seasonal trends of the O_2 emission at latitudes 65°S, 65°N, and the equator.

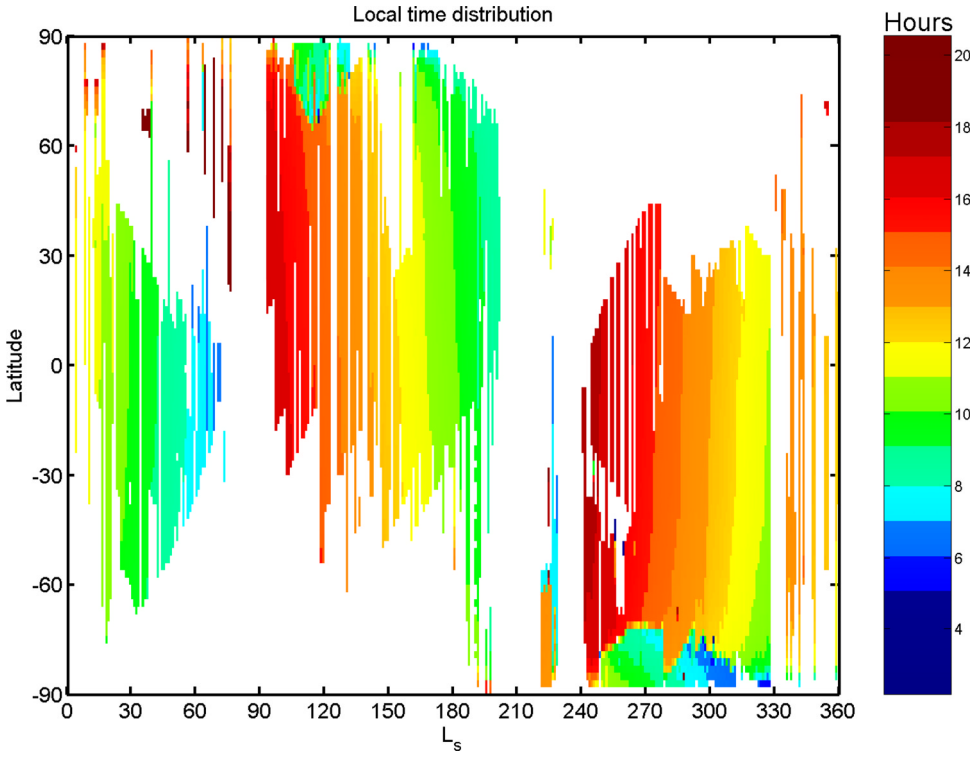

Figure 10. Map of local time for SPICAM nadir measurements.

observed by SPICAM at low latitudes is also consistent with these previous Earth-based observations.

[53] *Krasnopolsky* [2003] measured the latitudinal distribution of the O_2 dayglow for four heliocentric solar longitudes: L_s = 67°, 112°, 148°, 173°. All these measurements correspond to different Martian years (MY 23 through MY 26). In the designation proposed by *Clancy et al.* [2000] (Martian Year (MY) 1 = 11 April 1955), our data set corresponds to the end of MY 26, and covers almost the entire MY 27. We compared SPICAM observations (MY 27) for the same set of L_s in Figure 11. Ground-based measurements were averaged for the local time interval from 1100 to 1400, except the measurement at L_s = 67° taken at 1420. The error bars of our observations were calculated as described in section 4.4.

[54] The single SPICAM orbit available at L_s = 67° and 336°E of longitude indicates an O_2 emission 4 ± 1.1 MR at low latitudes. This is significantly smaller than the values obtained by *Krasnopolsky* [2003], who derived an emission of 7 MR in the 0°–20°S latitude band (MY 23). *Novak et al.* [2002] obtained from the same data sets even a larger value of 12 MR. We attribute the difference of our observations with the determinations of these authors to the variation of the O_2 emission with local time. Our measurements were taken in the morning (7 h) whereas the Earth-based observations presented here were obtained at 14 h20, near the diurnal maximum of the emission.

[55] At L_s = 112° SPICAM recorded four orbits corresponding to different longitudes. A comparison with the work of *Krasnopolsky* [1993] shows, in general, a better agreement within 2–4 MR for the longitude of 72°E close to ground-based observations. However, the increase in the O_2 emission observed by SPICAM from 20°N to 20°S by SPICAM was not recorded by *Krasnopolsky* [2003]. Again, this difference could be explained by differences in local time (15 h for SPICAM versus 11–14 h for the Earth-based measurements) and year-to-year variability.

[56] At L_s = 148° the local time of the SPICAM measurements (13 h) almost coincides with that of the ground-based observations. Two profiles are available for longitudes of 243°E and 144°E. At low-latitudes (20°S–30°N) our result for orbit 1305 (243°E) is two times below 2–3 MR detected with IRTF. However, for longitude of 144°E, which is closer to Krasnopolsky's observations the agreement is good within the error bars. However, a large increase in the O_2 emission at latitudes south of 40°S was not observed from the Earth. We note that there is no contamination by CO_2 ice for this orbit. The possible reasons for this discrepancy are discussed below.

[57] At L_s = 173° the local time of SPICAM observation is 11 h. In a broad low-latitude range we measure a low emission of ~1 MR, in good agreement with the Earth-based observations. At high northern latitudes our measurements indicate a sharp peak that largely exceeds the moderate increase observed by *Krasnopolsky* [2003]. The position of the peak changes from an orbit to an orbit. Orbits 1475 and 1476 were recorded at same local time but at different longitudes (83°E and 348°E). The peak maxima on these orbits have different amplitudes and are shifted by 5° of latitude.

[58] A colder middle atmosphere could decrease the atmospheric water content, and increase the ozone abundance. TES temperature measurements are available for MY 24, 25 and 26 [*Smith*, 2004], but unavailable for MY 27. The comparison of three Martian years shows weak variations in 0.5 mbar temperature on Mars at L_s = 148°

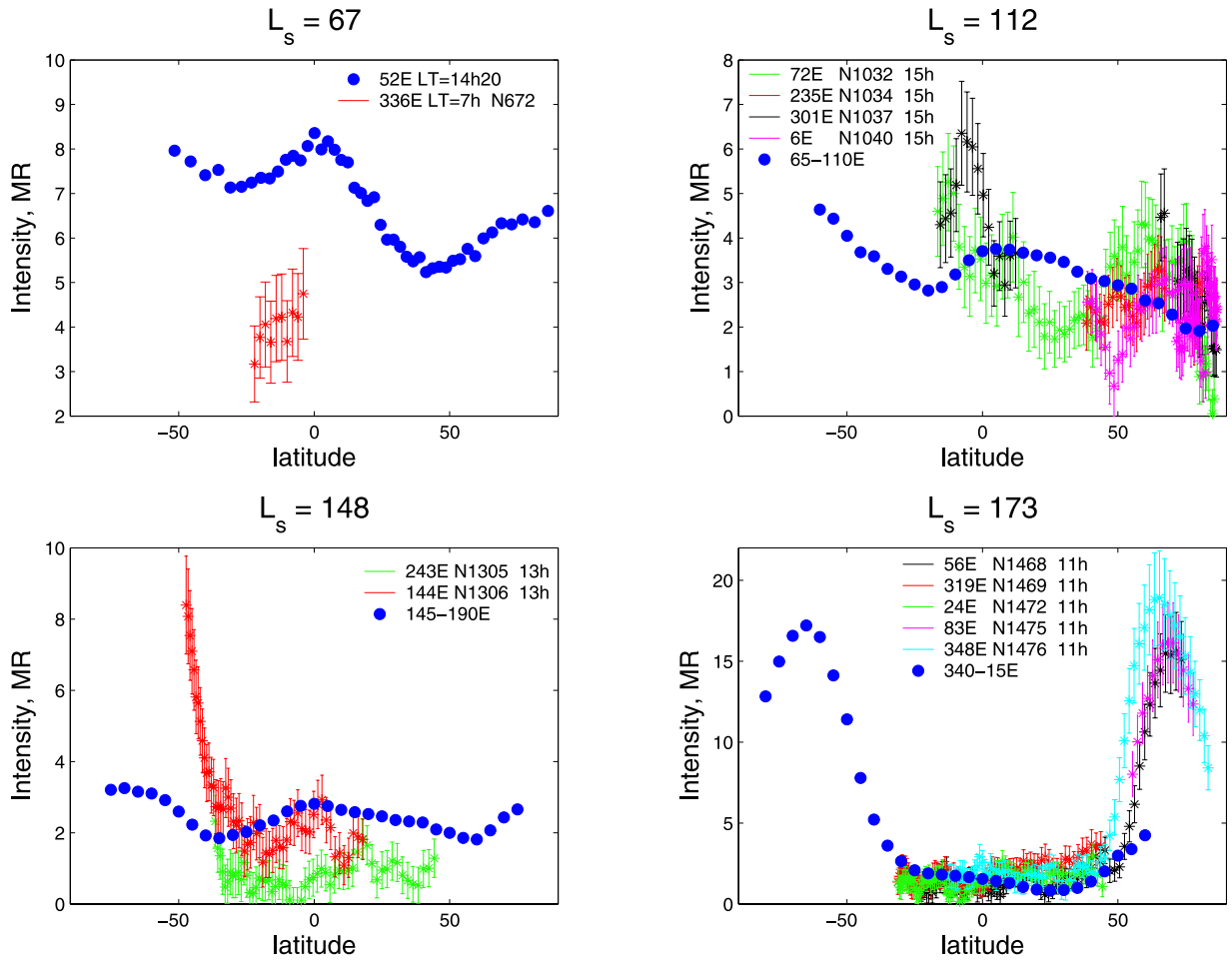

Figure 11. Comparison of SPICAM O_2 emission profiles with ground-based observations [*Krasnopolsky*, 2003] for four seasonal points. Circles are ground-based observations; asterisks with error bars are SPICAM data for different longitudes. N is an orbit number. Ground-based measurements at L_s = 112°, 148°, and 173° were averaged for the local time interval from 11h00 to 14h00.

above 40°S [*Smith*, 2004]. The south increase in our O_2 emission data at L_s = 148° coincides with the edge of the South polar cap, which already starts sublimating at this time. This process provokes the release of the dust into the atmosphere, and it may be highly irregular from year to year. The measurement by Krasnopolsky at L_s = 148° occurred at MY 25, and small enhancement of dust loading and atmospheric warming at 0.5 mbar level were observed at that time by TES [*Smith*, 2004]. It could increase the water and deplete the ozone in the middle atmosphere. Paradoxically, THEMIS atmospheric data, as communicated by *Smith* [2006] show a local enhancement of dust near L_s = 150° in the MY 27 in the equatorial region, which has never been observed before within the TES data set, and an enhanced atmospheric temperature at this moment extending up to the latitudes of 60°S.

[59] The observed differences might also relate to dynamics and interannual variability of the Martian ozone. At the southern latitudes, L_s = 148° and 50°S coincides with the edge of the South polar vortex with very large gradients in ozone (see *Lefevre et al*. [2004, Figure 1] or comparisons at L_s = 115° by *Fast et al.* [2006b]). At this time of year O_3 is a good tracer of dynamics. A big difference in O_3 amount (translated to O_2) can result from a slight difference in the position of the polar vortex at the time of the measurements. However, the map of the O_2 emission for full Martian disc at L_s = 148° [*Krasnopolsky*, 2003] does not show the evidence for large variability.

[60] At L_s = 173°, the MGCM also indicates that the high-latitude O_3 starts to increase very rapidly with time. The rapid change is apparent from SPICAM data set. Also, a difference in the onset of the O_3 increase from one year to another could largely explain the disagreement with *Krasnopolsky* [2003] at high northern latitudes.

[61] Besides the four published profiles *Krasnopolsky* [2003] mentioned a measurement on 19 Nov 1999 (L_s = 247°), when a very low value of the O_2 emission was detected. Similarly, *Farrell et al.* [2004] and *Novak et al.* [2005] did not detect the O_2 emission on 8–12 January 2002 (L_s = 306°) and on 11–15 January 2004 (L_s = 333°). The negative results at L_s = 247° and L_s = 306° are confirmed by SPICAM measurements. We have almost no data for L_s = 333° (early sporadic operations of Mars Express in January 2004), but subsequent orbits, and

measurements one Martian year later suggest no emission at this season below 35°N (see Figure 8).

7. Conclusions

[62] We have measured the $O_2(a^1\Delta_g)$ dayglow emission from near-IR spectra recorded by SPICAM instrument on board Mars Express from January 2004 (L_s = 330°) to November 2005 (L_s = 337°). This is the most complete set of observations to date of the O_2 dayglow on Mars. Observations of this emission are important for study of atmospheric ozone, and, more generally, for the Mars photochemistry. Such measurements, combined with measurements of total ozone column densities, can provide information on the altitude distribution of ozone in the atmosphere of Mars.

[63] In this study we did not attempt to evaluate the ozone column density from the O_2 emission intensity, as the procedure depends on poorly constrained a priori assumptions. Rather, we concentrated on the analysis of the seasonal distribution of O_2 dayglow emission as it is, and conclude the following.

[64] 1. The maximum O_2 emissions are observed in late winter/early spring at high latitudes of both hemispheres. The South hemisphere maximum (70°–80°S) reaches 30 MR and occurs at L_s = 185°–195°. North polar maximum (70°–80°N) is as much as 26 MR and occurs at L_s = 10°–20°.

[65] 2. The weakest emission is observed during summer in the Southern hemisphere. The emission intensity does not exceed 1–2 MR for this season.

[66] 3. The evolution of the O_2 emission at low latitudes (30°S–30°N) shows less contrast than in polar regions. However, there is evidence of a clear maximum of emission in the period L_s = 30°–120° centered on Mars aphelion. Mean intensities during the "aphelion season" are of the order of ~5–7 MR, in contrast with the 1–3 MR obtained for the rest of the year. This increase in emission is consistent with the larger O_3 concentrations which are measured at low latitudes near aphelion [*Clancy et al.*, 1999; *Fast et al.*, 2006a; *Perrier et al.*, 2006]. As predicted by three-dimensional model simulations, this results from the decrease in the altitude of the hygropause, leading to low abundances of hydrogen radicals and the subsequent growth of an O_3 layer above 20 km [*Lefevre et al.*, 2004].

[67] 4. Our measurements have been compared to ground-based O_2 dayglow observations; some latitude discrepancy can be in part explained by difference in local time, geographical coverage and year to year variability.

[68] Future work will include a combined analysis of the SPICAM nadir observations of the O_3 density from the UV Hartley continuum, the IR 1.27 μm O_2 emission, and the water vapor from 1.37 μm band to improve our knowledge about the ozone chemistry on Mars.

[69] **Acknowledgments.** The authors would like to thank our reviewers (Robert Novak and an anonymous referee) for careful revision and useful comments that help to improve appreciably this manuscript. We are grateful to V.A. Krasnopolsky for the ground-based O_2 emission data for comparison. Mars Express is a space mission from ESA (European Space Agency). We wish to express our gratitude to all ESA members who participated in this successful mission. We thank our collaborators at the three institutes for the design and the fabrication of the instruments (Service d'Aeronomie/France, BIRA/Belgium and IKI/Moscow). We thank also Astrium for the design and construction of the spacecraft. We thank CNES, Roskosmos, CNRS, Russian Academy of Sciences for financing SPICAM experiment. We wish to thank the Space Division of the Belgian Federal Science Policy Office for supporting this project through the ESA PRODEX program. The Russian team acknowledges RFBR grant 04-02-16856a. We are grateful to J.-C. Chauffray and Stephane Guibert at Service d'Aeronomie and A. Kiselev at IKI for the help with SPICAM IR calibration. We acknowledge E. Dimarellis and A. Reberac at Service d'Aeronomie for handling SPICAM operations.

References

Badger, R. M., A. C. Wright, and R. F. Whitlock (1965), Absolute intensities of the discrete and continuous absorption bands of oxygen gas at 1. 26 and 1. 065 μ and the radiative lifetime of the $^1\Delta_g$ state of oxygen, *J. Chem. Phys.*, *43*, 4345–4350.

Ball, S. M., and G. Hancock (1995), The relative quantum yields of $O_2(a^1\Delta_g)$ from the photolysis of ozone at 227 K, *Geophys. Res. Lett.*, *22*, 1213–1216.

Ball, S. M., G. Hancock, I. J. Murphy, and S. P. Rayner (1993), The relative quantum yields of $O_2(a^1\Delta_g)$ from the photolysis of ozone in the wavelength range 270 nm < λ < 329 nm, *Geophys. Res. Lett.*, *20*, 2063–2066.

Barth, C. A., and C. W. Hord (1971), Mariner ultraviolet spectrometer: Topography and polar caps, *Science*, *173*, 197–201.

Bertaux, J.-L., et al. (2001), The study of the Martian atmosphere from top to bottom with SPICAM light on Mars Express, *Planet. Space Sci.*, *48*, 1303–1320.

Bertaux, J.-L., et al. (2006), SPICAM on Mars Express: Observing modes and overview of UV spectrometer data and scientific results, *J. Geophys. Res.*, doi:10.1029/2006JE002690, in press.

Bibring, J.-P., et al. (2004), OMEGA: Observatoire pour la Mineralogie, l'Eau, les Galces et l'Activite, *Eur. Space Agency Spec. Publ.*, *ESA-SP 1240*, 37–50.

Clancy, R. T., and H. Nair (1996), Annual (perihelion-aphelion) cycles in the photochemical behavior of the global Mars atmosphere, *J. Geophys. Res.*, *101*, 12,785–12,790.

Clancy, R. T., M. J. Wolff, P. B. James, E. Smith, Y. N. Billawala, S. W. Lee, and M. Callan (1996), Mars ozone measurements near the 1995 aphelion: Hubble Space Telescope ultraviolet spectroscopy with the faint object spectrograph, *J. Geophys. Res.*, *101*, 12,777–12,783.

Clancy, R. T., M. J. Wolff, and P. B. James (1999), Minimal aerosol loading and global increases in atmospheric ozone during the 1996–1997 Martian northern spring season, *Icarus*, *138*, 49–63.

Clancy, R. T., B. J. Sandor, M. J. Wolff, P. R. Christensen, M. D. Smith, J. C. Pearl, B. J. Conrath, and R. J. Wilson (2000), An intercomparison of ground-based millimeter, MGS TES, and Viking atmospheric temperature measurements: Seasonal and interannual variability of temperatures and dust loading in the global Mars atmosphere, *J. Geophys. Res.*, *105*, 9553–9572.

Clancy, R. T., B. J. Sandor, and G. H. Moriarty-Schieven (2004), A measurement of the 362 GHz absorption line of Mars atmospheric H_2O_2, *Icarus*, *168*, 116–121.

DeMore, W. B., D. M. Golden, R. F. Hampson, M. J. Kurylo, C. J. Howard, A. R. Ravishankara, C. E. Kolb, and M. J. Molina (1997), Chemical kinetics and photochemical data for use in stratospheric modeling, evaluation 12, *JPL Publ.*, *97–4*, 269 pp.

Encrenaz, T., B. Bezard, T. K. Greathouse, M. J. Richter, J. H. Lacy, S. K. Atreya, A. S. Wong, S. Lebonnois, F. Lefevre, and F. Forget (2004), Hydrogen peroxide on Mars: Evidence for spatial and seasonal variations, *Icarus*, *170*, 424–429.

Farrell, A., T. Dunne, R. Novak, Y. Cabral, M. J. Mumma, and B. Bonev (2004), Seasonal mapping of ozone in the middle atmosphere of Mars, *Bull. Am. Astron. Soc.*, *36*, 15.

Fast, K., et al. (2006a), Ozone abundance on Mars from infrared heterodyne spectra. Acquisition, I., retrieval, and anticorrelation with water vapor, *Icarus*, *181*, 419–431.

Fast, K., T. Kostiuk, F. E. Espenak, T. Hewagama, M. F. A'Hearn, T. A. Livengood, S. Lebonnois, and F. Lefevre (2006b), Ozone abundance on Mars from infrared heterodyne spectra. II. Validating photochemical models, *Icarus*, *183*, 396–402.

Fiorenza, C., and V. Formisano (2005), A solar spectrum for PFS data analysis, *Planet. Space Sci.*, *53*, 1009–1016.

Forget, F., et al. (1999), Improved general circulation models of the Martian atmosphere from the surface to above 80 km, *J. Geophys. Res.*, *104*, 24,155–24,176.

Formisano, V., et al. (2005), The Planetary Fourier Spectrometer (PFS) onboard the European Mars Express mission, *Planet. Space Sci.*, *53*, 963–974.

Garcia Munoz, A., J. C. McConnell, I. C. McDane, and S. M. L. Melo (2005), Airglow on Mars: Some model expectations for the OH Meinel bands and the O2 IR atmospheric band, *Icarus*, *176*, 75–95.

Hansen, G. B. (2005), Ultraviolet to near-infrared absorption spectrum of carbon dioxide ice from 0.174 to 1.8 μm, *J. Geophys. Res.*, *110*, E11003, doi:10.1029/2005JE002531.

Jaquin, F., P. Gierasch, and R. Kahn (1986), The vertical structure of limb hazes in the Martian atmosphere, *Icarus*, *68*, 442–461.

Korablev, O., et al. (2006), SPICAM IR acousto-optic spectrometer experiment on Mars Express, *J. Geophys. Res.*, doi:10.1029/2006JE002696, in press.

Krasnopolsky, V. A. (1993), Photochemistry of the Martian atmosphere (mean conditions), *Icarus*, *101*, 313–332.

Krasnopolsky, V. A. (1997), Photochemical mapping of Mars, *J. Geophys. Res.*, *102*, 13,313–13,320.

Krasnopolsky, V. A. (2003), Mapping of Mars O_2 1. 27 μm dayglow at four seasonal points, *Icarus*, *165*, 315–325.

Krasnopolsky, V. A., and G. L. Bjoraker (2000), Mapping of Mars $O_2(^1\Delta)$ dayglow, *J. Geophys. Res.*, *105*, 20,179–20,188.

Lafferty, W. J., A. M. Solodov, C. L. Lugez, and G. T. Fraser (1998), Rotational line strengths and self-pressure-broadening coefficients for the 1.27–μm, a $a^1\Delta_g - X^3\Sigma^-_g$, v = 0–0 band of O_2, *Appl. Opt.*, *37*, 2264–2270.

Lane, A. L., C. A. Barth, C. W. Hord, and A. I. Stewart (1973), Mariner 9 Ultraviolet Spectrometer Experiment: Observations of ozone on Mars, *Icarus*, *18*, 102–108.

Lebonnois, S., E. Quemerais, F. Montmessin, F. Lefevre, J. L. Bertaux, and F. Forget (2006), Vertical distribution of ozone on Mars as measured by SPICAM/Mars Express using stellar occultation, *J. Geophys. Res.*, doi:10.1029/2005JE002643, in press.

Lefevre, F., S. Lebonnois, F. Montmessin, and F. Forget (2004), Three-dimensional modeling of ozone on Mars, *J. Geophys. Res.*, *109*, E07004, doi:10.1029/2004JE002268.

Mlynczak, M. G., and D. J. Nesbitt (1995), The Einstein coefficient for spontaneous emission of the $O_2(a^1\Delta_g)$ state, *Geophys. Res. Lett.*, *22*, 1381–1384.

Montmessin, F., E. Quemerais, J. L. Bertaux, O. Korablev, P. Rannou, and S. Lebonnois (2006), Stellar occultations at UV wavelengths by the SPICAM instrument: Retrieval and analysis of Martian haze profiles, *J. Geophys. Res.*, doi:10.1029/2005JE002662, in press.

Nair, H., M. Allen, A. D. Anbar, Y. L. Yung, and R. T. Clancy (1994), A photochemical model of the Martian atmosphere, *Icarus*, *111*, 124–150.

Newman, S. M., I. C. Lane, A. J. Orr-Ewing, D. A. Newnham, and J. Ballard (1999), Integrated absorption intensity and Einstein coefficients for the O_2 $a^1\Delta_g - X^3\Sigma^-_g$ (0,0) transition: A comparison of cavity ring-down and high resolution Fourier transform spectroscopy with a long-path absorption cell, *J. Chem. Phys.*, *110*, 10,749–10,757.

Novak, R. E., M. J. Mumma, M. A. DiSanti, N. Dello Russo, and K. Magee-Sauer (2002), Mapping of ozone and water in the atmosphere of Mars near the 1997 aphelion, *Icarus*, *158*, 14–23.

Novak, R. E., M. J. Mumma, S. Lee, L. Ivanov, B. Bonev, and G. Villanueva (2005), Mapping of D/H and Ozone in the Martian atmosphere near perihelion, *Bull. Am. Astron. Soc.*, *37*, 669.

Noxon, J. F., W. A. Traub, N. P. Carleton, and P. Connes (1976), Detection of O_2 airglow emission from Mars and the Martian ozone abundance, *Astrophys. J.*, *207*, 1025–1035.

Perrier, S., J. L. Bertaux, F. Lefevre, S. Lebonnois, O. Korablev, A. Fedorova, and F. Montmessin (2006), Global climatology of ozone on Mars from SPICAM/MEX UV measurements, *J. Geophys. Res.*, doi:10.1029/2006JE002681, in press.

Rothman, L. S., et al. (2005), The HITRAN 2004 Molecular Spectroscopic Database, *J. Quant. Spectrosc. Radiat. Transfer*, *96*, 139–204.

Sander, S. P., et al. (2003), Chemical kinetics and photochemical data for use in atmospheric studies, evaluation 14, *JPL Publ.*, 02–25.

Smith, M. D. (2004), Interannual variability in TES atmospheric observations of Mars during 1999–2003, *Icarus*, *167*, 148–165.

Smith, M. D. (2006), TES atmospheric temperature, aerosol optical depth, and water vapor observations 1999–2004, in *Second Workshop on Mars Atmosphere Modelling and Observations, Granada, Spain*, edited by F. Forget et al., p. 211, Lab. de Météorol. Dyn., Paris.

Traub, W. A., N. P. Carleton, P. Connes, and J. F. Noxon (1979), The latitude variation of O_2 airglow and O_3 abundance on Mars, *Atsrophys. J.*, *229*, 846–850.

Wehrbein, W. M., C. W. Hord, and C. A. Barth (1979), Mariner 9 Ultraviolet Spectrometer Experiment: Vertical distribution of ozone on Mars, *Icarus*, *38*, 288–299.

J.-L. Bertaux, F. Lefevre, and S. Perrier, Service d'Aéronomie, CNRS, BP 3, F-91371 Verrières-le-Buisson, France.

A. Fedorova and O. Korablev, IKI, 84/32 Profsoyuznaya, 117997 Moscow, Russia. (fedorova@spectrum.iki.rssi.ru)

A. Rodin, Moscow Institute of Physics and Technology, Institutsky dr. 9, 141700 Dolgoprudnyi, Russia.